Biomaterials 285 (2022) 121479

Contents lists available at ScienceDirect

Biomaterials

journal homepage: www.elsevier.com/locate/biomaterials

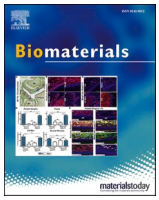

Flexible patch with printable and antibacterial conductive hydrogel electrodes for accelerated wound healing

Canran Wang [a,b,c,d,1], Xing Jiang [e,1], Han-Jun Kim [a,b,f,1], Shiming Zhang [a,b,g], Xingwu Zhou [a,b,h], Yi Chen [a,b,i,j], Haonan Ling [a,b,k], Yumeng Xue [l], Zhaowei Chen [a,m], Moyuan Qu [a,b,n], Li Ren [a,b,o,p], Jixiang Zhu [a,b,q,r], Alberto Libanori [a,b], Yangzhi Zhu [f], Heemin Kang [s], Samad Ahadian [a,b,f,t], Mehmet R. Dokmeci [a,b,f,t], Peyman Servati [u], Ximin He [c], Zhen Gu [a,v,w,x,y,z,aa], Wujin Sun [a,b,f,ab,**], Ali Khademhosseini [a,b,f,t,aa,ac,*]

[a] Department of Bioengineering, University of California, Los Angeles, Los Angeles, CA, 90095, USA
[b] Center for Minimally Invasive Therapeutics (C-MIT), California NanoSystems Institute, University of California, Los Angeles, Los Angeles, CA, 90095, USA
[c] Department of Materials Science and Engineering, University of California, Los Angeles, Los Angeles, CA, 90095, USA
[d] Andrew and Peggy Cherng Department of Medical Engineering, Division of Engineering and Applied Science, California Institute of Technology, Pasadena, CA, 91125, USA
[e] School of Nursing, Nanjing University of Chinese Medicine, Nanjing, 210023, China
[f] Terasaki Institute for Biomedical Innovation, Los Angeles, CA, 90064, USA
[g] Department of Electrical and Electronic Engineering, The University of Hong Kong, Hong Kong, SAR, China
[h] Department of Pharmaceutical Sciences, University of Michigan, Ann Arbor, MI, 48109, United States
[i] Bloomage Biotechnology Co., Ltd., Jinan, Shandong, 250101, China
[j] Bloomage Biotechnology Hainan Co.,Ltd., Haikou, Hainan, 571152, China
[k] Department of Mechanical and Aerospace Engineering, University of California, Los Angeles, Los Angeles, CA, 90095, USA
[l] State Key Laboratory of Solidification Processing, Center for Nano Energy Materials, School of Materials Science and Engineering, Northwestern Polytechnical University and Shaanxi Joint Laboratory of Graphene, Xi'an, 710072, China
[m] MOE Key Laboratory for Analytical Science of Food Safety and Biology, College of Chemistry, Fuzhou University, Fuzhou, 350108, China
[n] Stomatology Hospital, School of Stomatology, Zhejiang University School of Medicine, Zhejiang Provincial Clinical Research Center for Oral Diseases, Key Laboratory of Oral Biomedical Research of Zhejiang Province, Cancer Center of Zhejiang University, Hangzhou, 310006, China
[o] Key Laboratory for Space Bioscience and Biotechnology, School of Life Science, Northwestern Polytechnical University, Xi'an, Shanxi, 710072, China
[p] Research Center of Microfluidic Chip for Health Care and Environmental Monitoring, Yangtze River Delta Research Institute of Northwestern Polytechnical University, Taicang, Suzhou, Jiangsu, 215400, China
[q] Department of Biomedical Engineering, School of Basic Medical Sciences, Guangzhou Medical University, Guangzhou, 511436, China
[r] The Sixth Affiliated Hospital of Guangzhou Medical University, Qingyuan People's Hospital, Qingyuan, 511518, China
[s] Department of Materials Science and Engineering, Korea University, Seoul, 02841, Republic of Korea
[t] Department of Radiological Sciences, David Geffen School of Medicine, University of California, Los Angeles, Los Angeles, CA, 90095, USA
[u] Flexible Electronics and Energy Lab (FEEL), Department of Electrical and Computer Engineering, University of British Columbia, Vancouver, BC, V6T 1Z4, Canada
[v] College of Pharmaceutical Sciences, Zhejiang University, Hangzhou, 310058, China
[w] Department of General Surgery, Sir Run Run Shaw Hospital, School of Medicine, Zhejiang University, Hangzhou, 310016, China
[x] MOE Key Laboratory of Macromolecular Synthesis and Functionalization, Department of Polymer Science and Engineering, Zhejiang University, Hangzhou, 310027, China
[y] Zhejiang Laboratory of Systems & Precision Medicine, Zhejiang University Medical Center, Hangzhou, 311121, China
[z] Jinhua Institute of Zhejiang University, Jinhua, 321299, China
[aa] Jonsson Comprehensive Cancer Center, University of California, Los Angeles, Los Angeles, CA, 90095, USA
[ab] Department of Biological Systems Engineering, Virginia Tech, Blacksburg, VA, 24061, USA
[ac] Department of Chemical and Biomolecular Engineering, University of California, Los Angeles, Los Angeles, CA, 90095, USA

ARTICLE INFO

Keywords:
Wearable device

ABSTRACT

* Corresponding author. Terasaki Institute for Biomedical Innovation, Los Angeles, CA, 90064, USA.
** Corresponding author. Department of Biological Systems Engineering, Virginia Tech, Blacksburg, VA, 24061, USA.
E-mail addresses: sunw@vt.edu (W. Sun), khademh@terasaki.org (A. Khademhosseini).
[1] These authors contributed equally to this work.

https://doi.org/10.1016/j.biomaterials.2022.121479
Received 3 November 2021; Received in revised form 7 March 2022; Accepted 18 March 2022
Available online 14 April 2022

Electrical stimulation
Wound healing
Conductive hydrogel
Antibacteria

Electrical stimulation can facilitate wound healing with high efficiency and limited side effects. However, current electrical stimulation devices have poor conformability with wounds due to their bulky nature and the rigidity of electrodes utilized. Here, a flexible electrical patch (ePatch) made with conductive hydrogel as electrodes to improve wound management was reported. The conductive hydrogel was synthesized using silver nanowire (AgNW) and methacrylated alginate (MAA), with the former chosen as the electrode material considering its antibacterial properties, and the latter used due to its clinical suitability in wound healing. The composition of the hydrogel was optimized to enable printing on medical-grade patches for personalized wound treatment. The ePatch was shown to promote re-epithelization, enhance angiogenesis, mediate immune response, and prevent infection development in the wound microenvironment. *In vitro* studies indicated an elevated secretion of growth factors with enhanced cell proliferation and migration ability in response to electrical stimulation. An *in vivo* study in the Sprague-Dawley rat model revealed a rapid wound closure within 7 days compared to 20 days of usual healing process in rodents.

Credit author statement

Canran Wang: Methodology, Investigation, Validation, Writing - Original Draft. **Xing Jiang:** Methodology, Investigation, Validation, Writing - Original Draft. **Han-Jun Kim:** Methodology, Investigation, Validation, Writing - Original Draft. **Shiming Zhang:** Methodology, Investigation. **Xingwu Zhou:** Investigation. **Yi Chen:** Investigation. **Haonan Ling:** Investigation. **Yumeng Xu:** Investigation. **Zhaowei Chen:** Investigation. **Moyuan Qu:** Investigation. **Li Ren:** Investigation. **Jixiang Zhu:** Investigation. **Alberto Libanori:** Writing - Review & Editing. **Yangzhi Zhu:** Writing - Review & Editing. **Heemin Kang:** Writing - Review & Editing. **Samad Ahadian:** Writing - Review & Editing. **Mehmet R. Dokmeci:** Writing - Review & Editing. **Peyman Servati:** Writing - Review & Editing. **Ximin He:** Writing - Review & Editing. **Zhen Gu:** Writing - Review & Editing. **Wujin Sun:** Conceptualization, Methodology, Writing - Original Draft, Project administration. **Ali Khademhosseini:** Conceptualization, Supervision, Writing - Review & Editing, Funding acquisition.

1. Introduction

Wound healing is a common health burden that impacts millions of people, causing ~300,000 people hospitalized in the United States annually [1]. Surgeries, burns, abrasions, traumas, and superficial incisions can create wounds [2]. With improper treatments or health conditions like aging, diabetes, or vascular diseases, even a minor wound can develop into chronic wounds, which can remain nonhealing for years due to excessive inflammation, elevated reactive oxygen species (ROS) levels, persistent infections, or deficiency of stem cells [3–5]. By far, various methods have been developed for treating wounds, including growth factor-based drugs [6], microneedles [7], curcumin derivatives [8], wound debridement [9], wound dressings [10], negative pressure [11], and ultrasound [12,13]. Even with the various approaches, the average complete wound closure time for patients with pressure ulcers was over 12 weeks, where the lengthy healing process poses both physiological and financial burdens [14]. Accelerated healing process is highly desired not only in daily lives but also in emergency settings like wars and natural disasters, where resuming to normal activities is beneficial to both the patients and the society [15].

Electrical field (EF) stimulation can be an alternative for accelerating wound healing while limiting adverse effects associated with traditional therapies [16]. The delivery of EF at the wound site has been reported to guide the migration and proliferation of cutaneous cells, especially epithelial cells and fibroblasts, by activating ion channels and downstream transducing signals [17,18]. Additionally, EF-induced angiogenesis and immune modulation were observed in previous studies, both of which played essential roles in tissue remodeling [19–22]. Although current electrical stimulation devices, such as PosiFect RD™ DC device and Procellera® based on metallic electrodes, can contribute to the complete healing of 18-month intractable wounds within 12 weeks [23], they suffer from low mechanical conformability with the wound due to the bulkiness and rigidity of electrodes [24,25]. Despite severe side effects were not observed in the clinical trial with 7 patients, the imperfect conformability may cause skin inflammation and mental stress after long-term application in a larger study [26,27]. Additionally, wound conditions such as shapes and areas in various patients are different [28], wound patches that can be timely provided and customized are key to the efficacy of treatment.

Flexible and wearable electronics can directly interface with the human body. Physiological information, such as skin impedance and cardiovascular status, could be extracted [29,30], and therapeutic effects, such as neuromuscular regeneration, could be achieved [31]. Recently, remarkable efforts have been devoted to developing printable conductive material systems for wearable bioelectrodes that exploit the mechanical compliance at the skin-electronics interface as well as a simplified and precise patterning process [32,33]. Such electrode materials and fabrication approaches, if applied to wound healing, have the potential to advance clinical technologies for personalized wound care [34,35].

Here, we report a flexible electric patch (ePatch) with directly printed conductive hydrogel electrodes to deliver EF stimulations to the wound. Compared with existing electrodes for cutaneous wound healing [36–39], which are rigid and/or require dedicated fabrication technologies for patterning, ePatch has numerous advantages. For example, they have flexibility for the wearer's comfort, low-cost fabrication process without complicated equipment, printability for patterns with high resolution, simplicity in components, as well as biocompatibility and stability at the moist wound environment. These characteristics provide a promising solution to the challenges in the bioelectric field and personalized wound care. It was the first time that this conductive biomaterial system was formulated, containing two biocompatible components that have been widely used in U.S. Food and Drug Administration (FDA)-approved wound dressings. Silver nanowire (AgNW) can contribute to the conductivity and deliver the EF to the wound. Methacrylated alginate (MAA) can generate a matrix with biocompatibility, stability, printability, and mechanical compliance. Silver and its derivates, such as AgNW and silver nanoparticles, are great materials in wound dressings due to their excellent antibacterial capability. It is a highly desired property for treating wounds [40–43]. The morphology of AgNW further enables the electrode to maintain high conductivity even under strain [44]. Alginate, as a main component of clinical dressings, can keep optimal moisture levels at wound sites with good biocompatibility [45–47]. The presence of Ca^{2+} within the hydrogel can facilitate Ca^{2+}-induced cell proliferation and migration through Wnt/β-catenin and PI3K/Akt pathways, which synergize with electric simulations [48–50]. Ca^{2+} inside alginate can also contribute to haemostasis of wound healing [51]. The chemical modification of alginate, MAA, enhanced the stability of the electrode in an aqueous environment by forming a double-crosslinked network. To address the conformability issues, the shear-thinning property of the conducting hydrogel was optimized to enable its direct printing onto a wound patch, which is convenient for personalized wound treatment. Connected with

portable EF generators, our ePatch could address various challenges in treating wounds: 1) preventing bacterial infection; 2) accelerating cell migration and proliferation; 3) promoting blood vessel formation (Fig. 1). Such a simple but multifunctional biomaterial system is highly promising for facilitating wound healing in the clinic.

2. Results

2.1. Preparation and characterization of AgNW-MAA ink

Conductive hydrogel has been investigated for a variety of medical applications. They are generally composed of conductive nanomaterials and organic binders [52]. In our study, MAA was chosen as the organic binder, and AgNW was selected as the conductive nanomaterial [53,54]. AgNWs and MAA were synthesized and characterized by scanning electron microscope (SEM) and nuclear magnetic resonance (NMR), respectively (Fig. S1, S2). As shown in Fig. S1, the synthesized AgNWs had a large length-to-diameter ratio (~24 μm in length, and ~113 nm in diameter). A ~28% methacrylation of MAA was observed in NMR characterization (Fig. S2). Fourier transform infrared (FTIR) spectra were performed to validate the formation of double-crosslinked hydrogel matrices (Fig. S3). The obtained absorption peaks of double-crosslinked hydrogel indicated the formation of chelating structures and aliphatic chains from ionic and ultraviolet (UV) crosslinking.

A suitable AgNWs:MAA ratio is critical to enable shear-thinning features of the hydrogel. To optimize the composition, we tested the rheological properties of three different formulas (AgNWs and MAA in a weight ratio of 0:1 (3% w/v MAA), 10:3 (10% w/v AgNW, 3% w/v MAA), 20:3 (10% w/v AgNW, 1.5% w/v MAA), and 50:3 (10% w/v AgNW, 0.6% w/v MAA)). We chose the one with the highest viscosity when the low shear rate was applied to it, namely 10:3 AgNWs:MAA. This ratio had a viscosity of 237 Pa s at a shear rate of 0.1 s^{-1} and a viscosity less than 10 Pa s when the shear rate slightly increases, suggesting its capability of maintaining electrode integrity after printing (Fig. S4a) [52,55]. The rheology test also indicated that in response to shear stress increase, the liquid-like behavior (loss modulus, G″) exceeded solid-like behavior (storage modulus, G') (Fig. S4b). In order to assess the suitability of this hydrogel for high precision screen printing on paper, we also utilized it as ink to depict the logo "UCLA" (Fig. S5). The finally formulated hydrogel ink is shown in Fig. 2a. Our hydrogel ink stayed in the bottom of an upside-down bottle, indicating its high viscosity, while the inset image clearly showed its fluidity, which was consistent with the rheology test. An SEM image indicated a uniform mixture of the organic binder with AgNW after crosslinking (Fig. 2b). Since the silicone substrate was too hydrophobic for screen printing, we turned to mask-based printing to fabricate the ePatch (Fig. 2c, S6), and the side view of sectioned ePatch was presented in Fig. 2d. Our printed electrode had a thickness of approximately 5 μm, and the AgNWs network was uniformly mixed within the hydrogel, ensuring a high conductivity of 1.54×10^5 S m^{-1}.

2.2. Investigation of chemical and mechanical properties of ePatch

We subsequently investigated the chemical and mechanical stability of our printed electrodes. The printed lines submerged in deionized water retained good conductivity, and they are capable of lightning the bulbs, demonstrating that their conductivity can be maintained in the aqueous environment (Fig. S7). As presented in Fig. 2e, we tested the swelling property of the conductive hydrogel ink after dual-crosslinking. It was shown that the swelling ratio increased to 2.9 in the first 30 min of soaking the hydrogel in Dulbecco's phosphate-buffered saline (DPBS), and then it reached equilibrium. We also prepared calcium alginate with the same concentration of MAA hydrogel (i.e., 1.5% w/v) for comparison. The swelling ratio of the double-crosslinked hydrogel was slightly lower than calcium alginate (~3.5), suggesting better stability in the aqueous environment (Fig. 2e) [56]. We also soaked the electrode in DPBS and simulated wound fluid (SWF) for 6 days and monitored changes in resistance. After the incubation, the increases in resistance were less than 20% in both groups, indicating reasonable stability of the conductive hydrogel (Fig. 2f). These findings suggested that our ePatch could maintain its stability in wet environments such as those found in the proximity of interstitial fluid or those developed during perspiration at the wound site. To gain insight into the factors that affect the stability

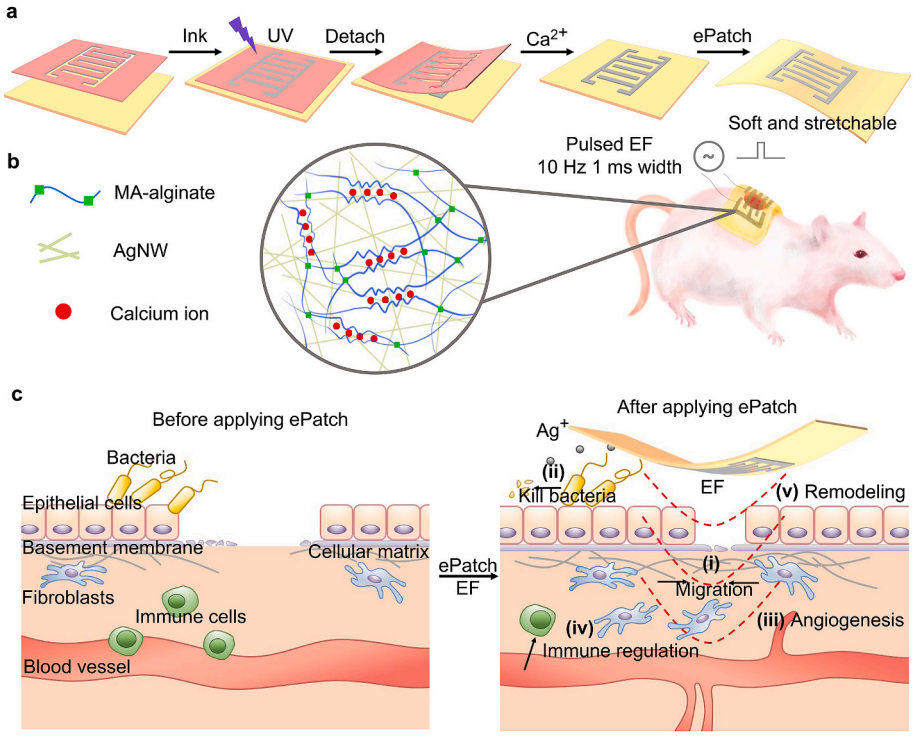

Fig. 1. (a) Schematic of the ePatch fabrication. A patterned mask was layered on the silicone substrate first. After depositing the conductive hydrogel ink and UV crosslinking, the mask was removed. Next, the $CaCl_2$ solution was added to generate a double-crosslinked network. (b) Schematic of AgNW-MAA ink formula and the double-crosslinked network. A uniform mixture of MAA and silver nanowire network system was generated. The ePatch was applied to a wound created on the back of a Sprague–Dawley rat with the indicated electric parameters. (c) Illustration of the biological activities of the ePatch during the healing process: (i) accelerating fibroblast migration and proliferation; (ii) suppressing bacteria growth; (iii) promoting angiogenesis; (iv) down-regulating immune cell activities; (v) improving re-epithelization and tissue remodeling.

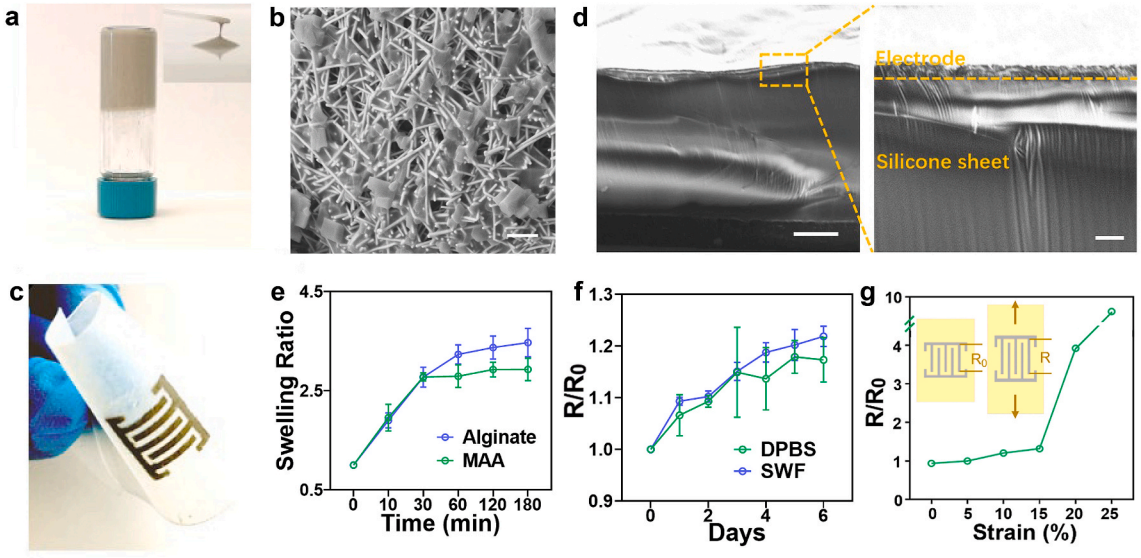

Fig. 2. (a) Photograph of the pre-crosslinked AgNW-MAA ink. (b) SEM image showing the AgNW wrapped inside MAA after crosslinking and lyophilization (scale bar = 1 μm). (c) Photograph of as-prepared ePatch. (d) SEM images of a cross-section of the fabricated electrode. The right image showed the magnified section of the left one. Scale bars represent 100 and 10 μm for left and right images, respectively. (e) Swelling of alginate and MAA-based double-crosslinked ink in DPBS and SWF for 6 days (n = 3, data represent mean ± SD). (f) Change of electrode resistance after soaking in DPBS (n = 3, data represent mean ± SD). Ratios of resistances at different time points (R) to time 0 (R_0) were calculated. (g) Resistance changes under strain ranging from 0 to 25%.

of ePatch, we compared printed lines in our formula that were made of 10% w/v AgNW, 3% w/v alginate. After submerging in deionized water for 12 and 24 h, AgNW release from the group with alginate was observed (Fig. S8). This result showed that the covalent modification of alginate enhanced the stability of ePatch in aqueous environment. To test the stretchability, Fig. 2g showed that there was only a slight increase in resistance in response to a strain of 15%. When strain was increased to 25%, the resistance increased abruptly, but the electrode still maintained good conductivity. Since the maximum strain rate of the human epidermis is around 15%, our ePatch provides sufficient strain tolerance to work continuously under the deformation of the skin [57]. To further demonstrate the improved mechanical compliance of a double-crosslinked network, we performed compressive tests (Fig. S9). The strain-stress curves showed that dual crosslinked hydrogel exhibited approximately 20- and 8-time higher compressive strengthens than single UV or calcium crosslinked hydrogels, respectively.

2.3. Assessment of the effects of EF stimulation on behaviors of NIH 3T3 fibroblasts

Next, we assessed ePatch's effectiveness in promoting wound healing *in vitro* on the surface of ePatch with or without EF (termed "ePatch w/EF" or "ePatch", respectively) (Fig. 3a). We chose NIH 3T3 fibroblasts as the model cell line since fibroblast cells play a crucial role in wound migration and tissue remodeling [58]. The biocompatibility of MAA was evaluated by culturing NIH 3T3 fibroblasts on MAA and then testing cell viability with Cell Counting Kit-8 (CCK-8) (Fig. S10). It was observed that MAA did not induce any significant cytotoxicity to the cells. The behavior of NIH 3T3 fibroblast cells in response to pulsed EF was investigated with parameters reported in previous studies of electrical simulation-based wound healing [19,38,59]. For the ePatch w/EF groups, our ePatch was connected to pulsed EF suppliers and placed below the cell culture modules. Under these experimental settings, *in vitro* scratch assay was performed to simulate the endogenous wound healing process via 2D cell culture. Fig. 3b and S11 showed that in the ePatch w/EF group, efficient migration of NIH 3T3 cells could be observed within 18 h, which was significantly faster than the control group (ePatch). Quantitative analysis also confirmed that the cells exposed to EF exhibited a significantly higher rate of migration (Fig. 3c). It was reported that cells could be aligned by EF, which could be regarded as an indicator of improvement in uniaxially directed migration [38,60]. To validate this property, we scattered cells with a much lower density than the scratch assay and applied the EF. In the group treated with ePatch, as the cells grew, they were randomly distributed, whereas the cells in the ePatch w/EF group showed an aligned cell growth pattern. A large portion of cells in the ePatch w/EF group aligned at a specific angle (Fig. 3d) [60]. For the ePatch group, a random distribution was observed with the orientation of -0.02 ± 0.04. While for the ePatch w/EF group, the orientation was -0.42 ± 0.05, indicating a perpendicular alignment. Similar results were observed in previous reports, suggesting that our EF parameter can guide cell alignment and migration in a specific direction [38,60–62]. The EF-induced alignment may be a result of cytoskeleton re-orientation during mitosis through Wnt/β-catenin and PI3K/Akt pathways [50,63–65]. LIVE/DEAD staining results further confirmed the viability of cells (Fig. 3d).

We tested cell proliferation by using CCK-8, monitoring the absorbance at 450 nm at different time points. With the increase of stimulation duration, the variance of absorbance between the two groups (ePatch and ePatch w/EF) became more significant, indicating enhanced cell viability and proliferation (Fig. 3e). ELISA assays were further conducted to test changes in cellular metabolism. Three growth factors, vascular endothelial growth factor-A (VEGF-A), transforming growth factor-beta (TGF-β), and epidermal growth factor (EGF), were tested in the supernatant of cell culture medium at 4 h, 12 h, 24 h, 48 h after applying the EF stimulations (Fig. 3f–h). Compared with the ePatch group, the expression of VEGF-A and TGF-β in cells with EF applied was significantly enhanced in the ePatch w/EF group. This confirmed that pulsed EF could affect cell signaling pathways to accelerate cell proliferation [66–68].

It is worth noting that the silicone substrate of ePatch can also benefit wound healing. Silicone substrate-based ePatch was shown to be non-adherent to cells, an essential characteristic of removable wound dressings [69,70]. To confirm this, we cultured fibroblast cells directly on the surface of the silicone substrate and observed that living cells did not attach to the substrate (Fig. S12a).

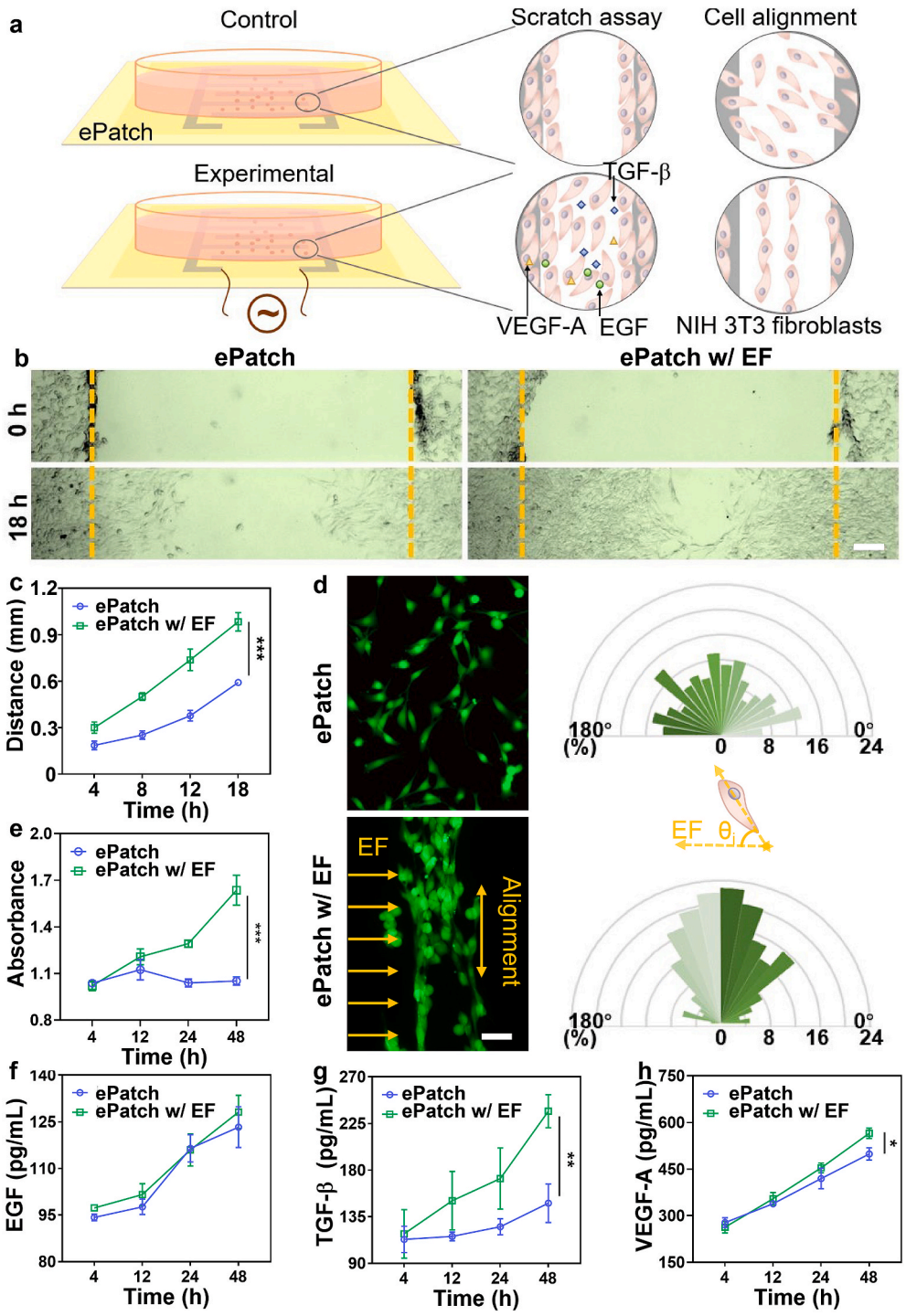

Fig. 3. (a) Schematic for testing cell behavior alterations in response to EF. NIH 3T3 fibroblast cells were treated with EF, and cells growing in the dish without EF were used as control. (b) Microscopic images of the scratch assay. Cells were stimulated with or without EF. (c) Cell migration distances at different time points after performing the scratch assay. (d) LIVE/DEAD staining of NIH 3T3 cells and quantification of cell angles in ePatch (upper) and ePatch w/EF groups (bottom) after applying EF for 24 h. Cells were aligned in lines indicated by the yellow arrows. The direction of the EF is also shown. Cell angles in ePatch and ePatch w/EF treated groups were quantitatively analyzed. (e) Cell proliferation was assessed by CCK-8 assay. (f) The secretion of EGF was monitored at different time points after applying EF. TGF-β (g) and VEGF-A (h) expressions in ePatch and ePatch w/EF groups were tested by ELISA. Scale bars represent 100 μm for (b) and 50 μm for (d). n = 3, data represent mean ± SD, $^{*}p < 0.05$, $^{**}p < 0.01$.

2.4. Evaluation of ePatch in accelerating wound healing in rats

To assess the therapeutic efficacies of ePatch *in vivo*, we used Sprague–Dawley rats as the animal model. The device was implanted into a full-thickness wound healing rat model [38]. As shown in Fig. 4a and S13, ePatch was directly applied onto the wound and connected to a Pulse Width Modulation (PWM) generator. The EF generation device was portable, wireless, small, and light-weighted (the average area was ~18 cm^2 and weight was ~15 g). It did not affect the physical activities of rats. In addition, the ePatch was soft and stretchable, thus providing a tight and conformed contact with the curved back of the rat without creating a gap between the wound and the electrode. Wounds were imaged at days 4 and 7, and the wound closure rate was compared to the original size of the wound (Fig. 4b and c). The control and ePatch groups showed no significant wound recovery on day 4. But in the ePatch w/EF group, the circular wound was closed in the vertical direction, and only a small wound portion remained. Similar to the *in vitro* migration assay where wound closure was facilitated only in the ePatch w/EF group. This rapid wound healing tendency was maintained throughout the experimental period (Day 7), and only a linear wound bed was observed in the ePatch w/EF treated group. In addition, the control group and the ePatch groups have round to wrinkle wound margins remained due to the irregular regeneration process, whereas the ePatch w/EF group has a wound margin that is almost linear. The wound area (%) remained were

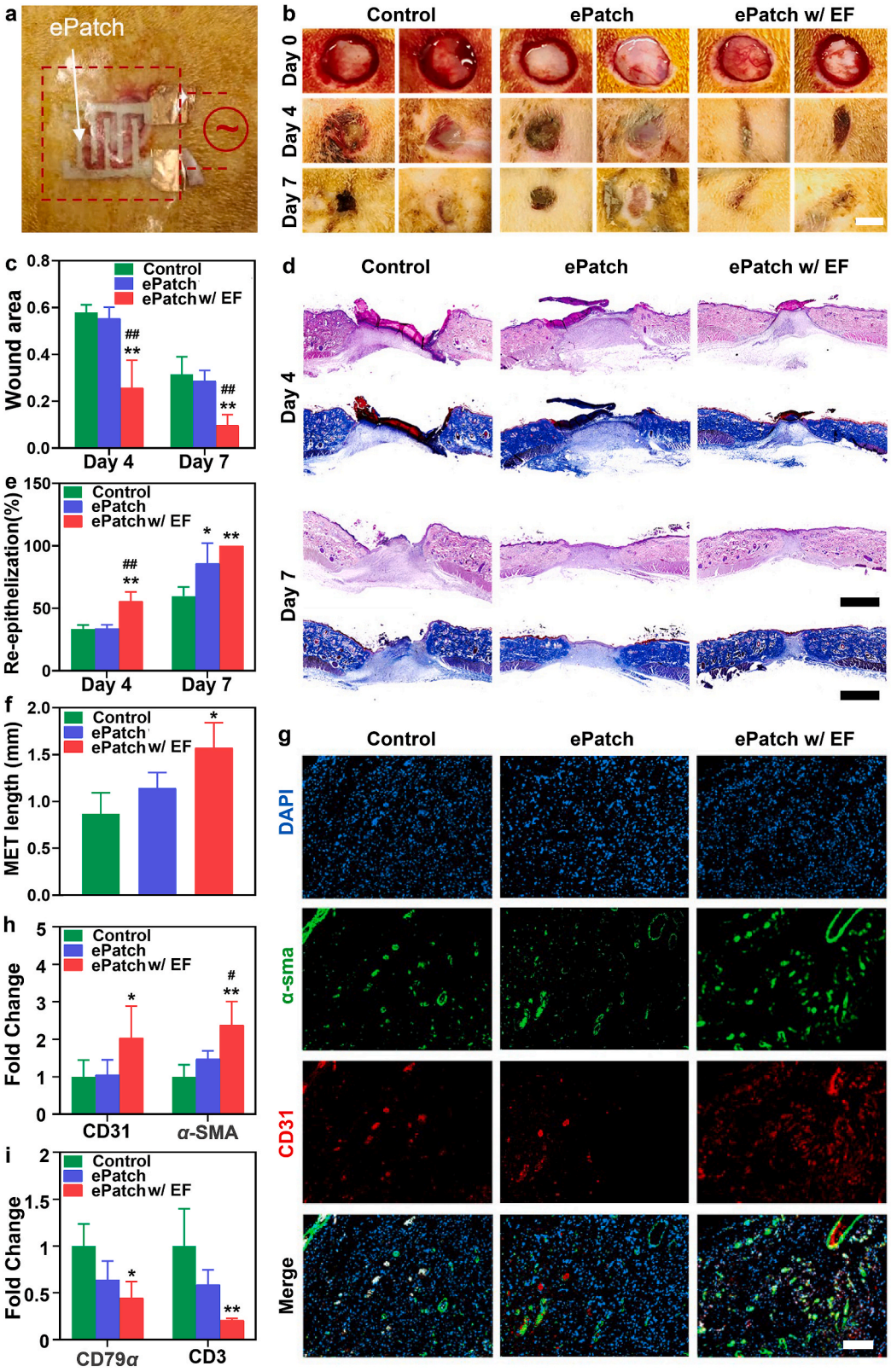

Fig. 4. (a) Photograph of the ePatch applied on the back of a Sprague–Dawley rat. (b) Optical images of wounds and residual wound areas at days 4 and 7 in different groups. (c) Analysis of wound areas remained open on days 4 and 7. (d) H&E and MT stainings of tissue sections of the wounds and adjacent skin areas (scale bar = 1 mm). (e–f) Analysis of the healing process, including re-epithelization percentage and MET length. Immunofluorescence observation (g) and quantification (h) of CD31 and α-SMA staining (scale bar = 100 μm). CD31 and α-SMA both indicated increased angiogenesis. (i) Quantification of CD79a and CD3 positive signals, biomarkers of B and T cells, respectively, at the wound beds in different groups. $^{*}p < 0.05$ and $^{**}p < 0.01$, compared with control group. $^{\#}p < 0.05$ and $^{\#\#}p < 0.01$, compared with ePatch group. n = 4, data represent mean ± SD.

57.9 ± 3.3% and 31.4 ± 7.5% on days 4 and 7, respectively, in the control group; 57.1 ± 4.0% and 28.6 ± 4.6% in the ePatch group; 25.7 ± 1.3% and 9.8 ± 4.5% in the ePatch w/EF group (Fig. 4c). It was notable that the wound in ePatch w/EF group was almost closed on day 4, while half of the wound remain unhealing in the control and ePatch group. These results indicated that ePatch w/EF not only improved wound regeneration but also minimized scarring and induced directional regeneration.

To further confirm the efficacy of ePatch in wound regeneration and tissue remodeling processes, we conducted Hematoxylin & Eosin (H&E) and Masson's Trichrome (MT) stainings of wound tissues (Fig. 4d–f). Low magnification histological analysis revealed that ePatch w/EF improved epidermal tissue migration in the wound bed compared to the other groups. The ePatch w/EF group showed faster wound regeneration throughout the experimental period compared to the other groups (Fig. 4b). In the MT staining, collagen proliferation and migration were prominent at day 4 in the ePatch w/EF group. On day 7, most of the dermal layer was remodeled to normal skin in the ePatch w/EF group with the regeneration of hair adnexa and deposition of collagen. The ePatch w/EF treated group demonstrated significantly more re-

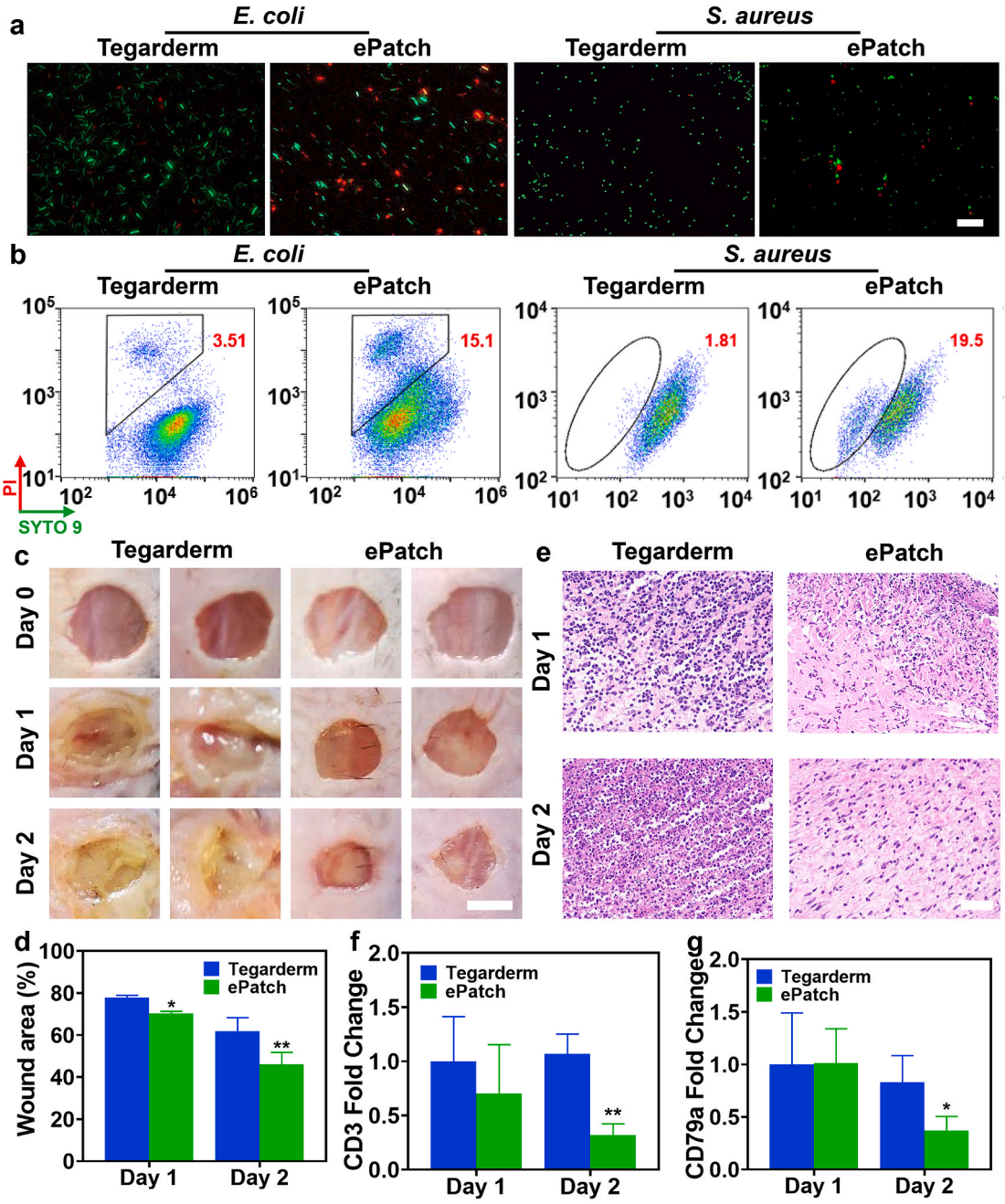

Fig. 5. (a) Fluorescent microscope imaging of BacLight LIVE/DEAD stained *E. coli* and *S. aureus* that have been cultured under different conditions for 2 h (scale bar = 100 μm). The green fluorescence stained intact cell membrane of bacteria, while the red fluorescence marked bacteria with damaged cell membrane. (b) Flow cytometry analysis of *E. coli* and *S. aureus* cultured under different conditions for 2 h. The gate showed bacteria with damaged cell membrane, and the numbers next to the gate indicated their percentages. (c) Photograph of *E. coli*- and *S. aureus*-infected mice skin wounds at different time points after bacterial inoculation (scale bar = 4 mm). (d) Quantitive analysis of the remaining wound area in each group (n = 3). (e) Quantitative analysis of MET length for different groups. (f) Representative H&E staining analysis at the wound sites (scale bar = 100 μm). (g) Quantification of inflammatory cells for different groups. $^{*}p < 0.05$, $^{**}p < 0.01$, and $^{**}p < 0.001$, n = 3, compared with Tegaderm group. $^{\#}p < 0.05$ and $^{\#\#}p < 0.01$, compared with ePatch group, data represent mean ± SD.

epithelialization (55.6 ± 7.6%, n = 4) than the other groups on day 4 (Control, 33.8 ± 3.1%; ePatch, 34.0 ± 2.9%) (Fig. 4d and e). Furthermore, the migrating epidermal tongue (MET) length of ePatch w/EF group was also significantly higher than that of the other groups (ePatch w/EF, 1.52 ± 0.3 mm; Control, 0.90 ± 0.3 mm; ePatch, 1.14 ± 0.2 mm) (Fig. 4f).

Finally, we verified angiogenesis and inflammatory cell infiltration *in vivo* using CD31/α-smooth muscle actin (α-SMA) (Fig. 4g and h) and CD3/CD79α (Fig. 4i and S14) immunofluorescence staining. At day 4, regions with angiogenesis, indicated by the CD31 positive (red) and α-SMA positive (green) tissues in immunofluorescence staining, were found to be more significantly enhanced in the ePatch w/EF group than the other groups. The percentages of CD31 or α-SMA positive areas were the highest in the ePatch w/EF group, as was the other wound healing indexes (wound area reduction%, re-epithelialization%, MET length), indicating an increased level of vessel formation at the early stage of healing (Fig. 4h) [71,72]. As a result of double immunofluorescence staining of the T-cell marker CD3 (red fluorescence) and B-cell marker CD79α (green fluorescence), ePatch w/EF was found to have less inflammation infiltration than the other groups at day 7 (Fig. 4i). These results indicated that the ePatch w/EF group passed the inflammation phase faster than the other groups, transitioning quickly to the migration and remodeling phases. In particular, for the ePatch w/EF group, the infiltration of T-cell and B-cell decreased by 79.5% and 55.4%, respectively, compared to the control group.

2.5. Verification of antibacterial efficiency of ePatch in vitro and in vivo

Silver nanocomposite has been reported to have a broad antibacterial spectrum, which is essential for a wound-healing patch [73]. To test the antibacterial capability of ePatch, both gram-negative and gram-positive bacteria *Escherichia coli* (*E. coli*) and *Staphylococcus aureus* (*S. aureus*) were cultured on the electrode side of the ePatch (Fig. 5 and S15). Bacteria were also cultured on glass slides (control) or Tegaderm. Tegarderm, serving as the negative control, has polyurethane-based adhesive for stable interfacing with irregular wound surfaces [74]. Tegarderm is a widely used air-permeable and water-proof dressing for wound care. It can protect the wound but does not have antibacterial properties. After electrical stimulation for 2 h, the LIVE/DEAD BacLight staining assay was conducted to investigate short-term antibacterial efficacy. Green fluorescence was detected in bacteria with intact cell membrane, demonstrating cell viability. Red fluorescence from propidium iodide (PI) and reduced green fluorescence from SYTO 9 marked bacteria with damaged cell membrane. It was observed that the ePatch caused significant damage to both *E. coli and S. aureus* (Fig. 5a) after 2 h of incubation, and flow cytometry results were consistent with this observation (Fig. 5b). After a 2 h incubation period with our electrodes, in the groups of ePatch and ePatch w/EF, the percentages of PI-positive *E. coli* were increased to 15.1% and 18.5%, respectively, indicating the presence of cellular injury. The percentage of SYTO 9-negative *S. aureus* increased after being incubated with the ePatch (control 2.54%, Tegaderm 1.81%, ePatch 19.5%, and ePatch w/EF 19.3%). These results showed that the proposed electrodes could efficiently inhibit bacterial growth in a very short time frame. The similar results between ePatch w/EF and ePatch groups indicated that the antibacterial efficacy was mostly exerted by the electrodes rather than EF. We also tested the long-term antibacterial properties of the ePatch by culturing *E. coli* and *S. aureus* under four different conditions (control, Tegaderm, ePatch, and ePatch w/EF) for 18 h, separately. *E. coli* and *S. aureus* were then sprayed on LB agar plates and incubated at 37 °C overnight. As presented in Fig. S16, no bacterial colony was formed in groups treated with ePatch, demonstrating the long-term antibacterial capabilities of ePatch.

In vivo antibacterial efficacy of the ePatch was further evaluated in an infected wound model. Full-thickness wounds with a diameter of 6 mm were created in the back of C57/BL6 mice (Fig. 5c). Mixed *E. coli* and *S. aureus* were sprayed on the wound bed. Since AgNW, instead of EF, is the main antibacterial component in the ePatch, the wounds were directly covered by ePatch without EF stimulations (ePatch group). In control groups, Tegaderm was applied to prevent further bacterial contamination from the surrounding environment. The wounds were imaged after 1 and 2 days. Visible infection was observed in the Tegaderm group, while wounds in the ePatch group were free from observable infection. Wound areas in the ePatch group were significantly smaller (42.04 ± 4.65% on day 2, n = 3) than the Tegaderm group (68.67 ± 5.21% on day 2; n = 3) (Fig. 5d). MET length also showed a similar trend: the ePatch group has a longer MET migration than the Tegaderm group (Fig. 5e). To better observe bacteria growth in the wound, wound exudates after patch treatment (days 1 and 2) were directly cultured on petri dishes (Fig. S17). The ePatch group generated significantly less bacterial colonies than the Tegaderm group. After 2 days of ePatch application, bacteria in wound exudate were almost undetectable, indicating excellent antibacterial efficacy. Staining of the cultured bacteria from wound exudates confirmed the presence of *E. coli* and *S. aureus* in both groups at day 1 (Fig. S18a). The infected wound tissue showed less bacteria in the ePatch group on day 2 (Fig. S18b). Then, we assessed inflammatory cell infiltrations in the wounds (Fig. 5f and g). The inflammatory cell densities decreased in the ePatch groups, indicating that inflammation can be mitigated by the ePatch along with inhibited bacteria growth (Fig. 5g).

Taken together, the *in vitro* and *in vivo* studies confirmed that the ePatch w/EF could be used to improve wound healing through enhanced cell migration and increased angiogenesis. It is worth noting that, even in the group applied with ePatch, the wound healing rate was elevated with inhibited immune response compared with the control group. We also demonstrated its capability of preventing gram-positive and negative bacterial infections *in vitro* and *in vivo*. These findings suggest that the ePatch can be directly used for wound healing treatment with good biocompatibility.

3. Conclusion

In summary, we have developed a flexible ePatch based on conductive hydrogel for accelerated wound healing. Conductive AgNW used in the hydrogel conferred antibacterial properties to the ePatch. Moreover, clinically used alginate hydrogel endowed the ePatch with good biocompatibility and printability. The double-crosslinked network enhanced the mechanical strength of the conductive hydrogel. By delivering EF to the wound, our ePatch was shown to boost the expression of growth factors by NIH 3T3 fibroblast cells, and the ePatch also lead to their enhanced proliferation and migration. Our *in vivo* model revealed that the ePatch could reduce wound healing time to 7 days, which was supposed to be 20 days if there was no treatment [75,76]. The promoted tissue remodeling outcome suggested a reduced degree of scar tissue formation. Compared to other AgNW-based wearable electric devices that are interfacing with healthy skin and/or rely on intricate fabrication processes [77–80], our ePatch can exploit double-crosslinked network to achieve high stability in wound environment and efficiency in accelerating wound healing. Our portable ePatch holds great promise to lower adverse impact from foreign implants as well, offering a new approach to assist wound treatment. Further optimization of this platform would benefit multidisciplinary research for various relevant diseases.

4. Materials and methods

4.1. Materials

Polyvinylpyrrolidone (PVP360, Mw ≈ 360,000 g mol^{-1}), silver nitrate, sodium chloride, sodium alginate (A2033, medium viscosity), 2-Aminoethyl methacrylate hydrochloride (AEMA, 900,652), polydimethylsiloxane (PHR1518, PDMS) and calcium chloride (C1016) were purchased from Sigma-Aldrich. Fibronectin and polyimide tapes were

supplied by Thermofisher Scientific.

4.2. Synthesis of the silver nanowire

AgNW was synthesized by reducing silver nitrate according to previous report. Briefly, 1 g of polyvinylpyrrolidone was mixed with 14 mg sodium chloride in 20 mL ethylene glycerol for 10 min. After heating in a 160 °C oil bath for 20 min, 10 mL 0.14 M silver nitrate was added very slowly at a speed of 10 mL h^{-1} using a syringe pump. The reaction was continued for an additional 30 min at 160 °C when the mixture turned greyish-green in color. The mixture was washed twice with acetone and three times with deionized water for purification. AgNW suspension was concentrated to 100 mg mL^{-1} (10 w/v%), which was approximately the maximum concentration of AgNW to maintain stability.

4.3. Synthesis of MA-Alginate

To modify alginate with AEMA, 100 mM MES buffer with pH = 6.5 was prepared. After dissolving 1 g sodium alginate in 100 mL MES buffer at 40 °C, 390 mg *N*-hydroxysuccinimide (NHS) and 840 mg -ethyl-3-(3-dimethylaminopropyl) carbodiimide (EDC) were sequentially added. The pH was adjusted to 8 and 672 mg of AEMA was added in 5 min. The mixture was allowed to further be mixed for 24 h at 40 °C. The mixture was then washed twice and dried under vacuum overnight. After that, the mixture was dialyzed for 3 days to remove residual NHS and EDC. It was then lyophilized. The sample was prepared at a concentration of 10 mg mL^{-1} in deuterium oxide for NMR to evaluate methacrylation. 3 w/v % MAA was chosen based on solubility.

4.4. Preparation of conductive inks and electrodes

The electrodes were patterned by printing on different substrates, such as glass slides and silicone sheets (CVS, USA). Masks for electrodes were prepared by laser cutting of tapes. Substrates were treated with oxygen plasma for 2 min (Plasma Etch, USA). We prepared inks with three different formulas (AgNWs and MAA in a weight ratio of 0:1 (3% w/v MAA), 10:3 (10% w/v AgNW, 3% w/v MAA), 20:3 (10% w/v AgNW, 1.5% w/v MAA), and 50:3 (10% w/v AgNW, 0.6% w/v MAA)) to find the optimal formulation. All prepared inks were then deposited on the masks above the substrates. Excessive ink was carefully removed by a glass slide, and the masks were detached from substrates. The optimized conductive ink (10:3) was chosen based on viscosity and shear-thinning properties as mentioned in the result section. The patterned ink was crosslinked with UV at an intensity of 6.9 mW cm^{-2} for 3 min. Then, the ink was soaked in 0.5 M calcium chloride solution for 10 min to generate a double-crosslinked network.

4.5. SEM imaging

For ePatch imaging, it was lyophilized and mounted on specimen holders with carbon adhesive tapes. It was sputtered with Au before imaging. For AgNW imaging, AgNW was dispersed in ethanol at a concentration of 1 w/v%. AgNW was dropped onto the carbon tapes on specimen holders and directly imaged after ethanol evaporation. All SEM images were collected from a Tescan Vega-3.

4.6. Rheology test

Rheological behaviors of different ink formulas (AgNWs:MAA w/v of 0:1, 10:3, 20:3, and 50:3) were measured by the Anton-Paar rheometer (MCR 302, Austria) at 25 °C with an 8 mm cone plate system and a 1 mm gap. The stress sweep test was run at a frequency of 1 Hz with oscillation stress of 0.1–100 Pa.

4.7. Stability test

Printed lines with a length of 1 cm and a width of 1 mm were prepared. To test the conductivity in an aqueous environment, we used a multimeter to measure the resistance of the printed lines before and after soaking them in DPBS for 1, 2, 3, 4, 5, and 6 days, respectively. To analyze the swelling ratio, 200 μL of the optimized conductive ink or the control group (calcium alginate, 1.5% w/v) were added in round PDMS molds with a diameter of 1 cm. After crosslinking ionically and chemically, all prepared hydrogel discs were lyophilized and weighed. The swelling ratio was calculated as: Swelling ratio = (Weight after soaking – Weight before soaking)/Weight before soaking × 100%. To evaluate the release of silver, we mixed AgNW with pure alginate or MAA with a ratio of 10:3 (10% w/v AgNW, 3% w/v pure alginate or MAA). The conductive inks were printed as lines with a length of 1 cm and a width of 1 mm. Photographs were taken after soaking the printed lines in deionized water for 12 and 24 h. SWF was prepared according to a previous report [81]. Briefly, 5.8 g sodium chloride, 3.4 g sodium hydrogen carbonate, 0.3 g potassium chloride, 0.3 g calcium chloride, 33.0 g bovine albumin, and 100 μL 30% hydrogen peroxide were dissolved in 1000 mL deionized water.

4.8. Stretchability test

To test the stretchability of ePatch, we mounted the whole ePatch on an Instron 300 LX. Resistances of the electrode were measured by a multimeter under different stresses (0%, 5%, 10%, 15%, 20%, and 25%)

4.9. Compressive test

Hydrogels (500 μL) were injected in round disc molds with a diameter of 1 cm and crosslinked with different approaches (UV 3 min/Ionic 10 min, UV 1.5 min/Ionic 10 min, UV 3 min, and Ionic 10 min). Then the hydrogels were mounted on an Instron 300 LX. The compressive strain was applied with a speed of 20%/min.

4.10. Electric stimulation

In all *in vitro* and *in vivo* experiments, the EF applied in the ePatch w/ EF group was continuous and in a parameter of 10 Hz with 1 ms pulse width.

4.11. Cell culture and proliferation test

NIH 3T3 fibroblasts (ATCC, CRL-1658) were cultured in Dulbecco's modified eagle medium (DMEM, Gibco, USA) supplemented with 10% bovine serum (BS, Gibco, USA) and 1% penicillin-streptomycin (Gibico, USA). 15 mm × 20 mm bottomless PDMS wells were assembled on the electrodes and sealed with half-cured PDMS to form cell culture chambers. The ePatch was then coated with Polyimide tapes with a thickness of 2 μm to enable cell adherence for migration and proliferation tests. The wells were incubated with 10 μg mL^{-1} fibronectin at 37 °C for 1 h and washed once with DPBS. We then seeded 1×10^5 cells with 2 mL media per well to achieve a cell density of approximately 400 cells/mm^2. After 12 h, EF was applied for cell viability and proliferation test. Cell viability was assessed by LIVE/DEAD Viability/Cytotoxicity kit (Invitrogen, USA) using protocols provided by the manufacturer. After incubating for 30 min, they were washed with DPBS. Cell proliferation was measured by CCK-8 (Cell counting kit-8) assay (Fisher Scientific, USA) and quantified by plate reader. For cell migration test, a confluent cell monolayer is required [82]. We performed a scratch assay with EF applied 2 days after cell seeding.

4.12. Biocompatibility test

To test the biocompatibility of MAA, we sprayed 1.5 w/v% MAA into

6-well plates with a volume of 200 μL/well. After crosslinking MAA as previously stated, we seeded 1×10^5 NIH 3T3 fibroblasts per well as well as 3 mL cell culture medium. Cells in the control group were directly cultured in untreated 6-well plates. CCK-8 assay was performed 4, 12, 24, and 48 h after culturing the cells.

4.13. Cell orientation analysis

To quantify the cell alignment along with the EF, we defined that for n cells, the orientation can be characterized as the average of $cos2\theta = \sum_{i=1}^{n} \frac{cos2\theta_i}{n}$, where the θ_i was the angle between the cell longest axis and EF. Thus, for cells that aligned perpendicular or parallel to EF, they will hold an orientation approximate to 1 or -1, respectively. While for randomly distributed cells, the orientation is near zero. For better visualization, cells were stained with LIVE/DEAD Viability/Cytotoxicity assay (Invitrogen, USA) based on protocols provided by the manufacturer before imaging.

4.14. ELISA assay

For TGF-β, VEGF-A, EGF ELISA tests (Invitrogen, USA), samples were collected from cell culture supernatant at various time points. For the pro-collagen ELISA test (Abcam, USA), samples were collected after lysing the cells. All ELISA tests were performed according to protocols recommended by vendors. The absorbance at 450 nm was measured by microplate readers.

4.15. Bacteria preparation

Escherichia coli (*E. coli*, ATCC BAA-2471) and *Staphylococcus aureus* (*S. aureus*, ATCC 29213) were used to analyze the antibacterial capabilities of ePatch *in vitro* and *in vivo*. Both bacteria were cultured in tryptic soy broth (TSB) medium at 37 °C. They were then diluted with DPBS and sprayed on LB Broth with agar plates (Sigma, USA) and cultured at 37 °C overnight for photograph.

4.16. Bacterial LIVE/DEAD assay

1 mL 1×10^7 CFU mL^{-1} bacterial suspension were cultured in 15 mm × 20 mm PDMS wells that were assembled with different substrates (glass slides, Tegaderm (3 M, USA), ePatch, or ePatch w/EF). The EF applied were the same as previously specified. After 2 h, we collected all the bacteria suspensions and centrifuged them. LIVE/DEAD BacLight bacterial viability kit (Thermofisher Scientific, USA) was used according to the protocol provided by the vendor. Microscopy (Zeiss, Germany) was then used to detect fluorescence. Flow cytometry was performed after cell staining. The samples were run on a BD FACSAria (BD Biosciences, USA) and data was processed and analyzed with FlowJo (FlowJo, USA).

4.17. In vivo therapeutic test

All animal experiments conducted were under protocols approved by the University of California, Los Angeles Animal Research Committee (UCLA ARC# 2018-003-01E). Purchased from Charles River Laboratories (CA, USA), twenty-four seven-week-old, Sprague-Dawley male rats with an average weight of 250–300 g were kept in a certified animal facility. Under general inhalable anesthesia (1.5% isoflurane in 100% O_2), a biopsy punch (Miltex, York, PA, USA) with a diameter of 8 mm was employed to make full-thickness excisional wounds on the middle of the back of the rats. Full-thickness skin, separated by Metzenbaum scissors, was cut off along the incision. Then, the wound was covered with experimental materials. 6 V 10 Hz pulsed EF with 1 ms width was applied continuously to the wound site. In total, 24 rats were divided into three groups randomly. The wound in the group with injury only (n = 4 each for days 4 and 7, control) was covered by medical-grade self-adhesive tapes (3 M, Northridge, CA, USA). In the ePatch (n = 4 each for days 4 and 7) or ePatch w/EF groups (n = 4 each for days 4 and 7), the wounds were covered with the electrode patch. For the ePatch w/EF group, the electrode patch was connected to the PWM generator. Rats were sacrificed using carbon dioxide for evaluating wound healing 4 and 7 days post-operation.

4.18. Histology evaluation

On days 0, 4, and 7, digital photographs of each wound were captured to analyze the wound contraction rate. ImageJ (National Institute of Health, USA) was used to assess the wound by observing the margin of the wound. The wound area (%) was calculated with the formula: 100% × (wound area at day 0 – wound area remaining wound)/(wound area at day 0). Immersed in a 10% formalin buffer (Leica Biosystems, USA), the wound tissue with surrounding unwounded skin was fixed. The samples then underwent a general procedure (dehydration, clearing, and embedding) for histopathological analysis. Paraffin sections with 4-μm thickness were processed with H&E stain. Histology images were collected on a Zeiss Axio Observer 5 inverted microscope (Carl Zeiss Microscopy, LLC, White Plains, NY, USA). AmScope image analysis software (AmScope, USA) was used to analyze quantitative data. The re-epithelialization percentage (%) was measured in the H&E-stained sections (n = 4). The re-epithelialization percentage was calculated as the following: re-epithelialization (%) = (epithelium coverage length/wound bed width) × 100%.

4.19. Immunofluorescence staining

Serial tissue sections were processed according to the standard immunofluorescence staining procedures, including deparaffinization, antigen-retrieval (citrated buffer, heat-induced), permeabilization (0.3% Triton PBST), and antigen blocking (goat serum, Cell Signaling Technology, USA). Then, as-prepared sections were incubated with antibodies, including mouse monoclonal α-SMA primary antibody (1:200; Novus Biologicals, USA), rabbit polyclonal CD31 primary antibody (1:200; Abcam, UK), rabbit monoclonal CD3 primary antibody (1:200; Abcam, UK), and mouse monoclonal CD79A primary antibody (1:200; Santa Cruz Biotechnology, USA). Then the sections were PBST-washed twice and incubated with secondary antibodies (goat anti-mouse Alexa 488, donkey anti-rabbit Alexa 555, ThermoFisher) at room temperature before counterstaining with DAPI. Fluorescent images were captured via Zeiss Axio Observer 5 Inverted Phase Contrast Fluorescent Microscope. Fluorescence intensity was analyzed and calculated using Image J (n = 4/group).

4.20. Infected wound model creation

E. coli and *S. aureus* suspension with an initial density of 2×10^8 CFU/mL were prepared and mixed with a ratio of 1:1 for inoculation. Twelve C57BL/6 mice were purchased and acclimatized for one week before the experiments. Following anesthesia by 1.5% isoflurane in 100% O_2, a biopsy punch with a diameter of 6 mm was used to create a full-thickness round wound on the dorsal face of the mouse. 100 μL of the bacterial suspension was sprayed on each wound surface for inoculation. Sterile swabs were used to harvest bacteria from wound exudates and draw a circle (diameter = 1 cm) on the surface of LB agar plates for bacterial culture. Three mice were used in each group.

4.21. Statistical analysis

Data analysis was all performed by using GraphPad Prism (Graphpad Software Inc., USA). The values represent the mean ± SD from three or more independent experiments. The statistical significance of

differences was assessed by Bonferroni posthoc paired comparisons tests and one-way ANOVA in histological evaluation. Otherwise, two-way ANOVA was employed. $*p < 0.05$, $**p < 0.01$, and $***p < 0.001$ were considered statistically significant.

Data availability

The experimental data required to reproduce the findings from this study will be made available to interested investigators upon request.

Declaration of competing interest

The authors declare that they have no known competing financial interests or personal relationships that could have appeared to influence the work reported in this paper.

Acknowledgment

The authors acknowledge funding from the National Institutes of Health (EB024403, EB023052, GM126831, and HL140618).

Appendix A. Supplementary data

Supplementary data to this article can be found online at https://doi.org/10.1016/j.biomaterials.2022.121479.

References

[1] T.N. Demidova-Rice, M.R. Hamblin, I.M. Herman, Acute and impaired wound healing: pathophysiology and current methods for drug delivery, part 1: normal and chronic wounds: biology, causes, and approaches to care, Adv. Skin Wound Care 25 (7) (2012) 304–314.
[2] Z. Iheozor-Ejiofor, K. Newton, J.C. Dumville, M.L. Costa, G. Norman, J. Bruce, Negative pressure wound therapy for open traumatic wounds, Cochrane Database Syst. Rev. 7 (7) (2018), Cd012522.
[3] Y. Xi, J. Ge, M. Wang, M. Chen, W. Niu, W. Cheng, Y. Xue, C. Lin, B. Lei, Bioactive anti-inflammatory, antibacterial, antioxidative silicon-based nanofibrous dressing enables cutaneous tumor photothermo-chemo therapy and infection-induced wound healing, ACS Nano 14 (3) (2020) 2904–2916.
[4] N. Mookherjee, M.A. Anderson, H.P. Haagsman, D.J. Davidson, Antimicrobial host defence peptides: functions and clinical potential, Nat. Rev. Drug Discov. 19 (5) (2020) 311–332.
[5] R.G. Frykberg, J. Banks, Challenges in the treatment of chronic wounds, Adv. Wound Care 4 (9) (2015) 560–582.
[6] M. Mochizuki, E. Güç, A.J. Park, Z. Julier, P.S. Briquez, G.A. Kuhn, R. Müller, M. A. Swartz, J.A. Hubbell, M.M. Martino, Growth factors with enhanced syndecan binding generate tonic signalling and promote tissue healing, Nat. Biomed. Eng. 4 (4) (2020) 463–475.
[7] X. Zhang, G. Chen, L. Sun, F. Ye, X. Shen, Y. Zhao, Claw-inspired microneedle patches with liquid metal encapsulation for accelerating incisional wound healing, Chem. Eng. J. 406 (2021) 126741.
[8] H. Lev-Tov, Small spice for big wounds: can curcumin close the gap? Sci. Transl. Med. 9 (385) (2017), eaan2776.
[9] A.L. Brundage, T.L. Crippen, J.K. Tomberlin, Methods for external disinfection of blow fly (Diptera: calliphoridae) eggs prior to use in wound debridement therapy, Wound Repair Regen. 24 (2) (2016) 384–393.
[10] M. Berthet, Y. Gauthier, C. Lacroix, B. Verrier, C. Monge, Nanoparticle-based dressing: the future of wound treatment? Trends Biotechnol. 35 (8) (2017) 770–784.
[11] M.L. Costa, Negative pressure wound therapy for open fractures-reply, JAMA 320 (16) (2018) 1709–1710.
[12] J.F. Holmes, K.M. Kelley, S.L. Wootton-Gorges, G.H. Utter, L.P. Abramson, J. S. Rose, D.J. Tancredi, N. Kuppermann, Effect of abdominal ultrasound on clinical care, outcomes, and resource use among children with blunt torso trauma: a randomized clinical trial, JAMA 317 (22) (2017) 2290–2296.
[13] L. Yu, R.J. Kronen, L.E. Simon, C.R.T. Stoll, G.A. Colditz, M.G. Tuuli, Prophylactic negative-pressure wound therapy after cesarean is associated with reduced risk of surgical site infection: a systematic review and meta-analysis, Am. J. Obstet. Gynecol. 218 (2) (2018) 200–210.e1.
[14] S. Wallenstein, H. Brem, Statistical analysis of wound-healing rates for pressure ulcers, Am. J. Surg. 188 (1) (2004) 73–78.
[15] C.K. Sen, G.M. Gordillo, S. Roy, R. Kirsner, L. Lambert, T.K. Hunt, F. Gottrup, G. C. Gurtner, M.T. Longaker, Human skin wounds: a major and snowballing threat to public health and the economy, Wound Repair Regen. 17 (6) (2009) 763–771.
[16] G. Thakral, J. Lafontaine, B. Najafi, T.K. Talal, P. Kim, L.A. Lavery, Electrical stimulation to accelerate wound healing, Diabet. Foot Ankle 4 (2013), https://doi.org/10.3402/dfa.v4i0.22081.
[17] M. Talikowska, X. Fu, G. Lisak, Application of conducting polymers to wound care and skin tissue engineering: a review, Biosens. Bioelectron. 135 (2019) 50–63.
[18] J. Li, F. Lin, Microfluidic devices for studying chemotaxis and electrotaxis, Trends Cell Biol. 21 (8) (2011) 489–497.
[19] B. Ferrigno, R. Bordett, N. Duraisamy, J. Moskow, M.R. Arul, S. Rudraiah, S. P. Nukavarapu, A.T. Vella, S.G. Kumbar, Bioactive polymeric materials and electrical stimulation strategies for musculoskeletal tissue repair and regeneration, Bioact. Mater. 5 (3) (2020) 468–485.
[20] S. Kargozar, F. Baino, S. Hamzehlou, M.R. Hamblin, M. Mozafari, Nanotechnology for Angiogenesis: Opportunities and Challenges, Chem Soc Rev, 2020.
[21] G. Opdenakker, J. Van Damme, J.J. Vranckx, Immunomodulation as rescue for chronic atonic skin wounds, Trends Immunol. 39 (4) (2018) 341–354.
[22] M. Phillipson, P. Kubes, The healing power of neutrophils, Trends Immunol. 40 (7) (2019) 635–647.
[23] M. Ashrafi, T. Alonso-Rasgado, M. Baguneid, A. Bayat, The efficacy of electrical stimulation in lower extremity cutaneous wound healing: a systematic review, Exp. Dermatol. 26 (2) (2017) 171–178.
[24] G. Yao, D. Jiang, J. Li, L. Kang, S. Chen, Y. Long, Y. Wang, P. Huang, Y. Lin, W. Cai, X. Wang, Self-activated electrical stimulation for effective hair regeneration via a wearable omnidirectional pulse generator, ACS Nano 13 (11) (2019) 12345–12356.
[25] A.K. Souza, T.R. Souza, L.M. Siqueira das Neves, G. de Paula Marcondes Ferreira Leite, S.B. Garcia, R. Roberto de Jesus Guirro, R.I. Barbosa, E. Caldeira de Oliveira Guirro, Effect of High Voltage Pulsed Current on the integration of total skin grafts in rats submitted to nicotine action, J. Tissue Viability 28 (3) (2019) 161–166.
[26] S. Roy, S. Prakash, S.S. Mathew-Steiner, P. Das Ghatak, V. Lochab, T.H. Jones, P. Mohana Sundaram, G.M. Gordillo, V.V. Subramaniam, C.K. Sen, Disposable patterned electroceutical dressing (PED-10) is safe for treatment of open clinical chronic wounds, Adv. Wound Care 8 (4) (2019) 149–159.
[27] T. Someya, M. Amagai, Toward a new generation of smart skins, Nat. Biotechnol. 37 (4) (2019) 382–388.
[28] B. Yang, J. Song, Y. Jiang, M. Li, J. Wei, J. Qin, W. Peng, F.L. Lasaosa, Y. He, H. Mao, J. Yang, Z. Gu, Injectable Adhesive self-healing multicross-linked double-network hydrogel facilitates full-thickness skin wound healing, ACS Appl. Mater. Interfaces 12 (52) (2020) 57782–57797.
[29] Y. Chang, L. Wang, R. Li, Z. Zhang, Q. Wang, J. Yang, C.F. Guo, T. Pan, First Decade of Interfacial Iontronic Sensing: from Droplet Sensors to Artificial Skins, Advanced Materials, Deerfield Beach, Fla., 2020, e2003464.
[30] S.R. Madhvapathy, H. Wang, J. Kong, M. Zhang, J.Y. Lee, J.B. Park, H. Jang, Z. Xie, J. Cao, R. Avila, C. Wei, V. D'Angelo, J. Zhu, H.U. Chung, S. Coughlin, M. Patel, J. Winograd, J. Lim, A. Banks, S. Xu, Y. Huang, J.A. Rogers, Reliable, low-cost, fully integrated hydration sensors for monitoring and diagnosis of inflammatory skin diseases in any environment, Sci. Adv. 6 (49) (2020).
[31] Y.S. Choi, Y.Y. Hsueh, J. Koo, Q. Yang, R. Avila, B. Hu, Z. Xie, G. Lee, Z. Ning, C. Liu, Y. Xu, Y.J. Lee, W. Zhao, J. Fang, Y. Deng, S.M. Lee, A. Vázquez-Guardado, I. Stepien, Y. Yan, J.W. Song, C. Haney, Y.S. Oh, W. Liu, H.J. Yun, A. Banks, M. R. MacEwan, G.A. Ameer, W.Z. Ray, Y. Huang, T. Xie, C.K. Franz, S. Li, J.A. Rogers, Stretchable, dynamic covalent polymers for soft, long-lived bioresorbable electronic stimulators designed to facilitate neuromuscular regeneration, Nat. Commun. 11 (1) (2020) 5990.
[32] C. Xu, Y. Yang, W. Gao, Skin-interfaced sensors in digital medicine: from materials to applications, Matter 2 (6) (2020) 1414–1445.
[33] M. Bariya, Z. Shahpar, H. Park, J. Sun, Y. Jung, W. Gao, H.Y.Y. Nyein, T.S. Liaw, L.-C. Tai, Q.P. Ngo, M. Chao, Y. Zhao, M. Hettick, G. Cho, A. Javey, Roll-to-Roll gravure printed electrochemical sensors for wearable and medical devices, ACS Nano 12 (7) (2018) 6978–6987.
[34] X. Yang, M. Sun, Y. Bian, X. He, A room-temperature high-conductivity metal printing paradigm with visible-light projection lithography, Adv. Funct. Mater. 29 (1) (2019) 1807615.
[35] S. Zhang, Y. Chen, H. Liu, Z. Wang, H. Ling, C. Wang, J. Ni, B. Çelebi-Saltik, X. Wang, X. Meng, H.-J. Kim, A. Baidya, S. Ahadian, N. Ashammakhi, M. R. Dokmeci, J. Travas-Sejdic, A. Khademhosseini, Room-temperature-formed PEDOT:PSS hydrogels enable injectable, soft, and healable organic bioelectronics, Adv. Mater. 32 (1) (2020) 1904752.
[36] C.R. Keese, J. Wegener, S.R. Walker, I. Giaever, Electrical wound-healing assay for cells in vitro, Proc. Natl. Acad. Sci. U. S. A 101 (6) (2004) 1554–1559.
[37] G. Thakral, J. Lafontaine, B. Najafi, T.K. Talal, P. Kim, L.A. Lavery, Electrical stimulation to accelerate wound healing, Diabet. Foot Ankle 4 (2013).
[38] Y. Long, H. Wei, J. Li, G. Yao, B. Yu, D. Ni, A.L.F. Gibson, X. Lan, Y. Jiang, W. Cai, X. Wang, Effective wound healing enabled by discrete alternative electric fields from wearable nanogenerators, ACS Nano 12 (12) (2018) 12533–12540.
[39] L. Mao, S. Hu, Y. Gao, L. Wang, W. Zhao, L. Fu, H. Cheng, L. Xia, S. Xie, W. Ye, Z. Shi, G. Yang, Biodegradable and electroactive regenerated bacterial cellulose/MXene (Ti(3) C(2) T(x)) composite hydrogel as wound dressing for accelerating skin wound healing under electrical stimulation, Adv. Healthc. Mater. 9 (19) (2020), e2000872.
[40] T. Cui, J. Yu, Q. Li, C.-F. Wang, S. Chen, W. Li, G. Wang, Large-scale fabrication of robust artificial skins from a biodegradable sealant-loaded nanofiber scaffold to skin tissue via microfluidic blow-spinning, Adv. Mater. (2020) 2000982, n/a(n/a).
[41] W.-C. Huang, R. Ying, W. Wang, Y. Guo, Y. He, X. Mo, C. Xue, X. Mao, A macroporous hydrogel dressing with enhanced antibacterial and anti-inflammatory capabilities for accelerated wound healing, Adv. Funct. Mater. 30 (21) (2020) 2000644.
[42] H. Chen, R. Cheng, X. Zhao, Y. Zhang, A. Tam, Y. Yan, H. Shen, Y.S. Zhang, J. Qi, Y. Feng, L. Liu, G. Pan, W. Cui, L. Deng, An injectable self-healing coordinative

hydrogel with antibacterial and angiogenic properties for diabetic skin wound repair, NPG Asia Mater. 11 (1) (2019) 3.
[43] T. Cui, J. Yu, Q. Li, C.-F. Wang, S. Chen, W. Li, G. Wang, Large-scale fabrication of robust artificial skins from a biodegradable sealant-loaded nanofiber scaffold to skin tissue via microfluidic blow-spinning, Adv. Mater. 32 (32) (2020) 2000982.
[44] P. Lee, J. Lee, H. Lee, J. Yeo, S. Hong, K.H. Nam, D. Lee, S.S. Lee, S.H. Ko, Highly stretchable and highly conductive metal electrode by very long metal nanowire percolation network, Adv. Mater. 24 (25) (2012) 3326–3332.
[45] B. ter Horst, G. Chouhan, N.S. Moiemen, L.M. Grover, Advances in keratinocyte delivery in burn wound care, Adv. Drug Deliv. Rev. 123 (2018) 18–32.
[46] Y. Shen, G. Xu, H. Huang, K. Wang, H. Wang, M. Lang, H. Gao, S. Zhao, Sequential release of small extracellular vesicles from bilayered thiolated alginate/polyethylene glycol diacrylate hydrogels for scarless wound healing, ACS Nano 15 (4) (2021) 6352–6368.
[47] Y. Zhu, Z. Ma, L. Kong, Y. He, H.F. Chan, H. Li, Modulation of macrophages by bioactive glass/sodium alginate hydrogel is crucial in skin regeneration enhancement, Biomaterials 256 (2020) 120216.
[48] S. Li, D. Lu, J. Tang, J. Min, M. Hu, Y. Li, Y. Liu, L. Wang, C. Liu, L. Hong, Electrical stimulation activates fibroblasts through the elevation of intracellular free Ca^{2+}: potential mechanism of pelvic electrical stimulation therapy, BioMed Res. Int. 2019 (2019) 7387803.
[49] Y. Sun, B. Mayers, T. Herricks, Y. Xia, Polyol synthesis of uniform silver nanowires: a plausible growth mechanism and the supporting evidence, Nano Lett. 3 (7) (2003) 955–960.
[50] C.-C. Xue, M.-H. Li, L. Sutrisno, B.-B. Yan, Y. Zhao, Y. Hu, K.-Y. Cai, Y. Zhao, S.-H. Yu, Z. Luo, Bioresorbable Scaffolds with Biocatalytic Chemotherapy and in Situ Microenvironment Modulation for Postoperative Tissue Repair, Advanced Functional Materials n/a(n/a) 2008732.
[51] J. Yu, H. Su, S. Wei, F. Chen, C. Liu, Calcium content mediated hemostasis of calcium-modified oxidized microporous starch, J. Biomater. Sci. Polym. Ed. 29 (14) (2018) 1716–1728.
[52] J. Liang, K. Tong, Q. Pei, A water-based silver-nanowire screen-print ink for the fabrication of stretchable conductors and wearable thin-film transistors, Adv. Mater. 28 (28) (2016) 5986–5996.
[53] W.Y. Ng, A. Migotto, T.S. Ferreira, L.B. Lopes, Monoolein-alginate beads as a platform to promote adenosine cutaneous localization and wound healing, Int. J. Biol. Macromol. 102 (2017) 1104–1111.
[54] M. Li, H. Li, X. Li, H. Zhu, Z. Xu, L. Liu, J. Ma, M. Zhang, A bioinspired alginate-gum Arabic hydrogel with micro-/nanoscale structures for controlled drug release in chronic wound healing, ACS Appl. Mater. Interfaces 9 (27) (2017) 22160–22175.
[55] R. Rudež, J. Pavlič, S. Bernik, Preparation and influence of highly concentrated screen-printing inks on the development and characteristics of thick-film varistors, J. Eur. Ceram. Soc. 35 (11) (2015) 3013–3023.
[56] A. Mandal, A.V. Boopathy, L.K.W. Lam, K.D. Moynihan, M.E. Welch, N.R. Bennett, M.E. Turvey, N. Thai, J.H. Van, J.C. Love, P.T. Hammond, D.J. Irvine, Cell and fluid sampling microneedle patches for monitoring skin-resident immunity, Sci. Transl. Med. 10 (467) (2018) eaar2227.
[57] Y. Liu, M. Pharr, G.A. Salvatore, Lab-on-Skin: a review of flexible and stretchable electronics for wearable health monitoring, ACS Nano 11 (10) (2017) 9614–9635.
[58] S. Mahmoudi, E. Mancini, L. Xu, A. Moore, F. Jahanbani, K. Hebestreit, R. Srinivasan, X. Li, K. Devarajan, L. Prélot, C.E. Ang, Y. Shibuya, B.A. Benayoun, A.L.S. Chang, M. Wernig, J. Wysocka, M.T. Longaker, M.P. Snyder, A. Brunet, Heterogeneity in old fibroblasts is linked to variability in reprogramming and wound healing, Nature 574 (7779) (2019) 553–558.
[59] M.R. Cho, H.S. Thatte, R.C. Lee, D.E. Golan, Integrin-dependent human macrophage migration induced by oscillatory electrical stimulation, Ann. Biomed. Eng. 28 (3) (2000) 234–243.
[60] S.J. Bunn, A. Lai, J. Li, DC electric fields induce perpendicular alignment and enhanced migration in schwann cell cultures, Ann. Biomed. Eng. 47 (7) (2019) 1584–1595.
[61] M. Zhao, H. Bai, E. Wang, J.V. Forrester, C.D. McCaig, Electrical stimulation directly induces pre-angiogenic responses in vascular endothelial cells by signaling through VEGF receptors, J. Cell Sci. 117 (Pt 3) (2004) 397–405.
[62] T. Zajdel, G. Shim, L. Wang, A. Rossello-Martinez, D. Cohen, SCHEEPDOG: programming electric cues to dynamically herd large-scale cell migration, Cell Syst. 10 (2020) 506–514, e3.
[63] Y. Li, G. Huang, X. Zhang, L. Wang, Y. Du, T.J. Lu, F. Xu, Engineering cell alignment in vitro, Biotechnol. Adv. 32 (2) (2014) 347–365.
[64] M. Zhao, B. Song, J. Pu, T. Wada, B. Reid, G. Tai, F. Wang, A. Guo, P. Walczysko, Y. Gu, T. Sasaki, A. Suzuki, J.V. Forrester, H.R. Bourne, P.N. Devreotes, C. D. McCaig, J.M. Penninger, Electrical signals control wound healing through phosphatidylinositol-3-OH kinase-γ and PTEN, Nature 442 (7101) (2006) 457–460.
[65] E. Finkelstein, W. Chang, P.H. Chao, D. Gruber, A. Minden, C.T. Hung, J. C. Bulinski, Roles of microtubules, cell polarity and adhesion in electric-field-mediated motility of 3T3 fibroblasts, J. Cell Sci. 117 (Pt 8) (2004) 1533–1545.
[66] Z. Zhang, X. Zhang, D. Zhao, B. Liu, B. Wang, W. Yu, J. Li, X. Yu, F. Cao, G. Zheng, Y. Zhang, Y. Liu, TGF-β1 promotes the osteoinduction of human osteoblasts via the PI3K/AKT/mTOR/S6K1 signalling pathway, Mol. Med. Rep. 19 (5) (2019) 3505–3518.
[67] M. Zhao, J. Pu, J.V. Forrester, C.D. McCaig, Membrane lipids, EGF receptors, and intracellular signals colocalize and are polarized in epithelial cells moving directionally in a physiological electric field, Faseb. J. : Off. Publ. Feder. Am. Soc. Exp. Biol. 16 (8) (2002) 857–859.
[68] H. Zhuang, W. Wang, R.M. Seldes, A.D. Tahernia, H. Fan, C.T. Brighton, Electrical stimulation induces the level of TGF-beta 1 mRNA in osteoblastic cells by a mechanism involving calcium/calmodulin pathway, Biochem. Biophys. Res. Commun. 237 (2) (1997) 225–229.
[69] W.M. Shaw, H. Yamauchi, J. Mead, G.-O.F. Gowers, D.J. Bell, D. Öling, N. Larsson, M. Wigglesworth, G. Ladds, T. Ellis, Engineering a model cell for rational tuning of GPCR signaling, Cell 177 (3) (2019) 782–796, e27.
[70] A.R. Unnithan, A. Ghavami Nejad, A.R.K. Sasikala, R.G. Thomas, Y.Y. Jeong, P. Murugesan, S. Nasseri, D. Wu, C.H. Park, C.S. Kim, Electrospun zwitterionic nanofibers with in situ decelerated epithelialization property for non-adherent and easy removable wound dressing application, Chem. Eng. J. 287 (2016) 640–648.
[71] Y.X. Lv, S. Zhong, H. Tang, B. Luo, S.J. Chen, L. Chen, F. Zheng, L. Zhang, L. Wang, X.Y. Li, Y.W. Yan, Y.M. Pan, M. Jiang, Y.E. Zhang, L. Wang, J.Y. Yang, L.Y. Guo, S. Y. Chen, J.N. Wang, J.M. Tang, VEGF-A and VEGF-B coordinate the arteriogenesis to repair the infarcted heart with vagus nerve stimulation, cellular physiology and biochemistry, Int. J. Exp. Cell. Physiol. Biochem. Pharmacol. 48 (2) (2018) 433–449.
[72] J. Liang, Q. Cheng, J. Huang, M. Ma, D. Zhang, X. Lei, Z. Xiao, D. Zhang, C. Shi, L. Luo, Monitoring tumour microenvironment changes during anti-angiogenesis therapy using functional MRI, Angiogenesis 22 (3) (2019) 457–470.
[73] C.Y. Chen, H. Yin, X. Chen, T.H. Chen, H.M. Liu, S.S. Rao, Y.J. Tan, Y.X. Qian, Y. W. Liu, X.K. Hu, M.J. Luo, Z.X. Wang, Z.Z. Liu, J. Cao, Z.H. He, B. Wu, T. Yue, Y. Y. Wang, K. Xia, Z.W. Luo, Y. Wang, W.Y. Situ, W.E. Liu, S.Y. Tang, H. Xie, Ångstrom-scale silver particle-embedded carbomer gel promotes wound healing by inhibiting bacterial colonization and inflammation, Sci. Adv. 6 (43) (2020).
[74] S.L. Levengood, A.E. Erickson, F.-C. Chang, M. Zhang, Chitosan-Poly(caprolactone) nanofibers for skin repair, J. Mater. Chem. B 5 (9) (2017) 1822–1833.
[75] M.A. Prestes, C.A.P.M. Ribas, J.M. Ribas Filho, L.B. Moreira, A.B.W. Boldt, E. V. Brustolin, L.S. Castanho, J.A. Bernardi, F.C. Dias, Wound healing using ionic silver dressing and nonocrystalline silver dressing in rats, Acta Cir. Bras. 27 (2012) 761–767.
[76] A. Gupta, G.K. Jain, R. Raghubir, A time course study for the development of an immunocompromised wound model, using hydrocortisone, J. Pharmacol. Toxicol. Methods 41 (4) (1999) 183–187.
[77] C. Lim, Y. Shin, J. Jung, J.H. Kim, S. Lee, D.-H. Kim, Stretchable conductive nanocomposite based on alginate hydrogel and silver nanowires for wearable electronics, Apl. Mater. 7 (3) (2018), 031502.
[78] Q. Han, Y. Chen, W. Song, M. Zhang, S. Wang, P. Ren, L. Hao, A. Wang, S. Bai, J. Yin, Fabrication of agarose hydrogel with patterned silver nanowires for motion sensor, Bio-Des. Manuf. 2 (4) (2019) 269–277.
[79] F. Ershad, A. Thukral, J. Yue, P. Comeaux, Y. Lu, H. Shim, K. Sim, N.-I. Kim, Z. Rao, R. Guevara, L. Contreras, F. Pan, Y. Zhang, Y.-S. Guan, P. Yang, X. Wang, P. Wang, X. Wu, C. Yu, Ultra-conformal drawn-on-skin electronics for multifunctional motion artifact-free sensing and point-of-care treatment, Nat. Commun. 11 (1) (2020) 3823.
[80] C. Wang, E. Shirzaei Sani, W. Gao, Wearable Bioelectronics for Chronic Wound Management, Advanced Functional Materials n/a(n/a) 2111022.
[81] C. Bradford, R. Freeman, S.L. Percival, In vitro study of sustained antimicrobial activity of a new silver alginate dressing, J. Am. Col. Certif. Wound Spec. 1 (4) (2009) 117–120.
[82] C.-C. Liang, A.Y. Park, J.-L. Guan, In vitro scratch assay: a convenient and inexpensive method for analysis of cell migration in vitro, Nat. Protoc. 2 (2) (2007) 329–333.